ARL-TR-10337 • MAY 2026

Spatially Resolved Laser-Induced Air Shock from Energetic Materials (SR-LASEM) Measurements, Part II: Printed Ammonium Perchlorate-Copper(II) Oxide Deposits

by Jennifer L. Gottfried

NOTICES

Disclaimers

The findings in this report are not to be construed as an official Department of the Army position unless so designated by other authorized documents.

Citation of manufacturer's or trade names does not constitute an official endorsement or approval of the use thereof.

Destroy this report when it is no longer needed. Do not return it to the originator.

ARL-TR-10337 ● MAY 2026

Spatially Resolved Laser-Induced Air Shock from Energetic Materials (SR-LASEM) Measurements, Part II: Printed Ammonium Perchlorate-Copper(II) Oxide Deposits

Jennifer L. Gottfried
DEVCOM Army Research Laboratory

REPORT DOCUMENTATION PAGE

1. REPORT DATE	2. REPORT TYPE	3. DATES COVERED	
		START DATE	END DATE
May 2026	Technical Report	3/30/2026	4/6/2026

4. TITLE AND SUBTITLE
Spatially Resolved Laser-Induced Air Shock from Energetic Materials (SR-LASEM) Measurements, Part II: Printed Ammonium Perchlorate-Copper(II) Oxide Deposits

5a. CONTRACT NUMBER	5b. GRANT NUMBER	5c. PROGRAM ELEMENT NUMBER
5d. PROJECT NUMBER	**5e. TASK NUMBER**	**5f. WORK UNIT NUMBER**

6. AUTHOR(S)
Jennifer L. Gottfried

7. PERFORMING ORGANIZATION NAME(S) AND ADDRESS(ES)	8. PERFORMING ORGANIZATION REPORT NUMBER
DEVCOM Army Research Laboratory ATTN: FCDD-RLA-WA Aberdeen Proving Ground, MD 21005	ARL-TR-10337

9. SPONSORING/MONITORING AGENCY NAME(S) AND ADDRESS(ES)	10. SPONSOR/MONITOR'S ACRONYM(S)	11. SPONSOR/MONITOR'S REPORT NUMBER(S)

12. DISTRIBUTION/AVAILABILITY STATEMENT
DISTRIBUTION STATEMENT A. Approved for public release: distribution unlimited.

13. SUPPLEMENTARY NOTES
ORCID: Jennifer L. Gottfried, 0000-0002-1282-1928

14. ABSTRACT
Spatially resolved laser-induced air shock from energetic materials (SR-LASEM) measurements were performed on printed ammonium perchlorate (AP)-copper(II) oxide (CuO) samples. The surface adhesion, sample homogeneity, batch-to-batch reproducibility, and influence of sample thickness on the energy release were investigated. No significant statistical differences in fast energy release were observed from batch to batch for the same number of deposition layers. Increasing the number of deposition layers reduced the contribution of the substrate to the emission spectra, decreased the shot-to-shot variability in the emission signals, increased the characteristic laser-induced shock velocities, and increased the amount of material blowoff surrounding the laser-material interaction region (thus increasing the intensity and duration of the post-plasma combustion). The optimal number of deposition layers to minimize substrate ablation (and subsequent energy content dilution), enhance the signal-to-noise ratios for sample emission lines, and minimize excess sample blowoff (maximizing the number of shots per printed sample) was four layers.

15. SUBJECT TERMS
printed energetic materials, ammonium perchlorate, AP, copper(II) oxide, CuO, laser-induced air shock from energetic materials, LASEM, Weapons Sciences

16. SECURITY CLASSIFICATION OF:			17. LIMITATION OF ABSTRACT	18. NUMBER OF PAGES
a. REPORT	b. ABSTRACT	C. THIS PAGE		
UNCLASSIFIED	UNCLASSIFIED	UNCLASSIFIED	UU	30

19a. NAME OF RESPONSIBLE PERSON	19b. PHONE NUMBER *(Include area code)*
Jennifer L. Gottfried	(520) 691-6002

STANDARD FORM 298 (REV. 5/2020)
Prescribed by ANSI Std. Z39.18

Contents

List of Figures

List of Tables

Acknowledgments

Printed samples were provided by Profs. Mortaza Saeidi and Joe Kalman (California State University, Long Beach).

1. Introduction

In Part I of this series,[1] the spatially resolved laser-induced air shock from energetic materials (SR-LASEM) method—based on the original LASEM method[2] and differing only in sample configuration—was used on a plasma-synthesized material directly deposited on a substrate to demonstrate the influence of deposit location along the substrate on energetic content and chemical composition. Here in Part II, SR-LASEM was directly applied to printed samples of ammonium perchlorate (AP) with 1 wt% copper(II) oxide (CuO) produced by collaborators at California State University, Long Beach. AP is a strong oxidizer commonly used for composite solid propellants. Metal oxides such as CuO alter the combustion properties of AP.[3] CuO acts as a particularly efficient catalyst that significantly reduces the temperature at which the AP decomposes, increasing the burning rate and energy release—thus improving the overall performance and efficiency of the solid propellant.[4]

Additive manufacturing (i.e., 3D printing) offers significant advantages for producing energetic materials, including unprecedented design freedom for complex geometries, tailored performance for specific applications, significant reduction in lead times, and on-demand localized production (reducing inventory and supply chain reliance).[5,6] The disadvantages of additive manufacturing include limited materials suitable for printing, poor layer adhesion, the presence of voids and defects that compromise structural integrity and performance, material inhomogeneity, and batch-to-batch variation. By directly interrogating the printed sample with a pulsed laser, SR-LASEM enables identification of many of these printing issues that may contribute to inconsistent performance—particularly material inhomogeneity and batch-to-batch variation. For this study, four sets of AP + CuO samples were used to investigate the adhesion of the sample to the substrate, the influence of the sample thickness on the material performance, the homogeneity of the printed samples, and the batch-to-batch consistency.

2. Experimental

2.1 Sample

The printing material consisted of 1 wt% CuO added to an AP-methanol solution with polyvinylpyrrolidone (PVP) added in a 2:1 ratio with respect to the CuO.[7] The PVP enhances the dispersion, adhesion, viscosity, and stability of the energetic ink. The sample thicknesses consisted of 1, 2, 4, or 8 layers and ranged from approximately 30 to 150 µm thick. Three identical square (~10 mm) deposits of

each layer thickness were printed on a microscope slide to enable evaluation of batch-to-batch consistency (denoted A-C, as shown in Figure 1). Microscope images were acquired on a dark background once the samples were received at U.S. Army Combat Capabilities Development Command (DEVCOM) Army Research Laboratory (ARL) (Figure 2). These images demonstrate variations in the layer thickness across each individual square deposit, as well as inhomogeneity in the CuO dispersion (brown streaks).

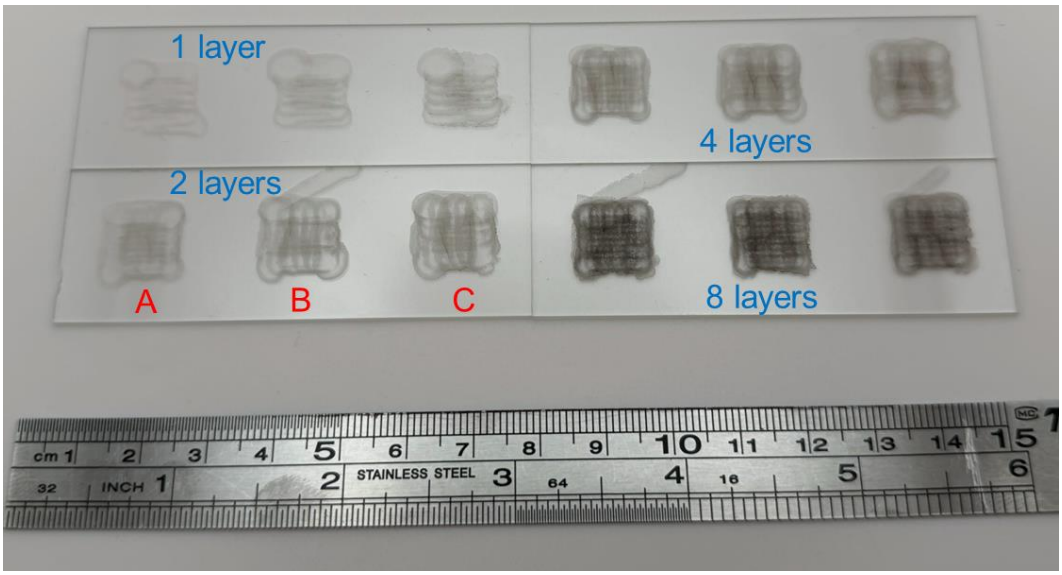

Figure 1. The as-prepared AP + CuO samples.[8]

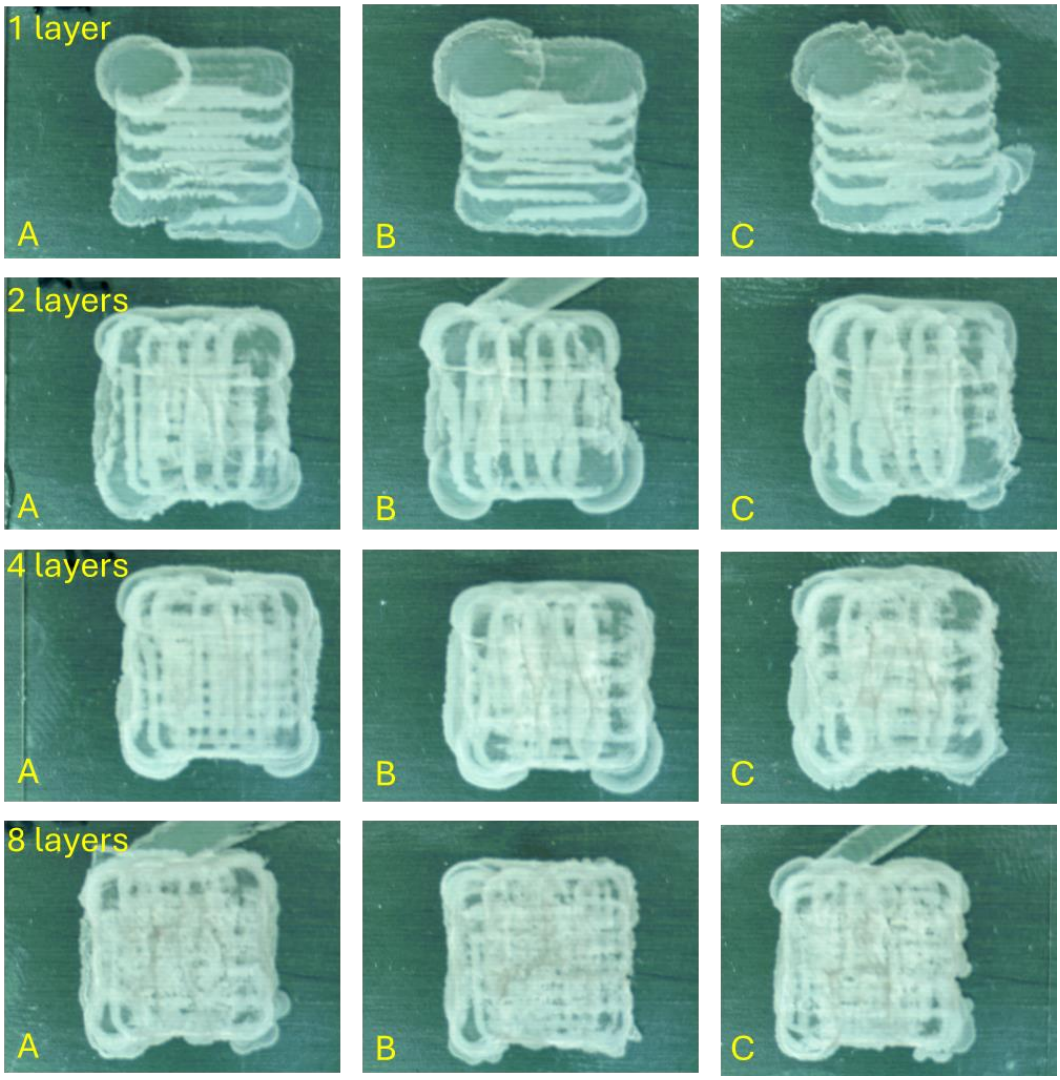

Figure 2. Microscope images of the as-received AP + CuO samples.

2.2 LASEM

The LASEM-420 system used for this work has been described previously.[2] Custom MATLAB code was used to analyze the shock front positions in the high-speed schlieren videos and calculate the performance parameters.[9,10] These included the characteristic laser-induced shock velocity (y-intercept of the fifth order polynomial fit to the shock velocity vs. time), Dewey shock velocity (value of the Dewey fit to the shock velocities vs. time at 13 μs), and energy added to the plasma by the exothermic reactions of the plasma (based on a combination Sedov–Taylor and drag model fit).[2] The shock front positions in the first five frames were measured manually; shock front positions in the subsequent frames, determined by the edge-detection algorithm, were rounded down to the nearest pixel.[11] The statistical significance of the calculated performance parameters was analyzed by

additional custom MATLAB code.[12] What differentiates SR-LASEM from conventional LASEM is that the pulsed laser directly ablates the printed sample as prepared (in contrast to a typical LASEM sample preparation where the loose powder sample is affixed to double-sided tape prior to the measurement) and the location of each laser shot is noted to enable location-based analyses.

Additional diagnostic data was collected beyond the high-speed schlieren videos of the laser-induced shock wave expansion into the air above the sample. An echelle spectrograph with an intensified charge-coupled device (ICCD) detector (Catalina Scientific SE200 with Apogee detector) was used to monitor the laser-induced plasma emission following laser excitation; spatially integrated light from the plasma was focused into the spectrometer's fiber-optic cable using a UV-collimating lens. The spectrometer has broad wavelength coverage from 200 to 1000 nm with an average resolution of 0.02 nm. The gain of the ICCD was set to 900, and the spectrometer trigger was delayed 1.5 μs after the laser fired to avoid the continuum emission. A gate width of 10 μs was selected to cover the duration of the shock wave passage through the plasma region. A free-space, 10-MHz IR-sensitive (900–1700 nm) photoreceiver (New Focus Model 2053) was pointed at the laser–material interaction region to monitor the time-resolved post-plasma combustion emission. A total of 27–29 laser shots were saved for each sample thickness using squares A and B (Table 1).

Table 1. No. laser shots saved per sample.

Sample	No. laser shots (square A)	No. laser shots (square B)
1 layer	15	12
2 layers	17	12
4 layers	16	12
8 layers	13	15

3. Results

Figure 3 shows microscope images from square A of each sample before and after SR-LASEM. The 1-layer samples show uneven deposits with significant partially transparent sections. The laser ablation spot size for each laser shot (numbered in yellow) is consistent with the diameter of the focused laser at the substrate surface. The sample was manually moved after each laser shot; for better precision in laser shot spacing, a laser pointer could be added to the experimental setup to direct placement of each laser shot—but at the cost of increased time for data collection. The adhesion of the material to the substrate and size of the printed square was sufficient to enable the collection of 12–16 laser shots per square. The two-layer sample has fewer transparent areas but is still unevenly deposited. As with the one-

layer sample, the mass removal for each laser shot is generally consistent with the laser diameter; however, additional material was ejected from the slide near some shots. The four-layer samples are more evenly deposited, with more significant mass removal surrounding the laser beam for some shots. The eight-layer samples had the fewest transparent areas, but significant material blowoff occurred with each laser shot. Increasing the adhesion between sample layers could decrease the amount of material ejected with each laser shot.

Figure 4 shows example snapshots from the high-speed schlieren video for each sample. The laser propagates from right to left and the subsequent laser-induced plasma and shock waves propagate from left to right (into the air above the sample surface). Emission from the plasma is visible in the first frame; each subsequent frame is 2.38 μs after the last (shutter exposure is 369 ns). Unlike the other samples, green emission from copper (Cu) dominates the plasma emission for the eight-layer sample. In addition to the strong laser-induced shock wave, the expansion of the heated gas products is shown in the schlieren images. Ejected particles blown off the sample surface by the refracted shock wave appear as dark objects in the eight-layer sample plume, along with increased turbulence.

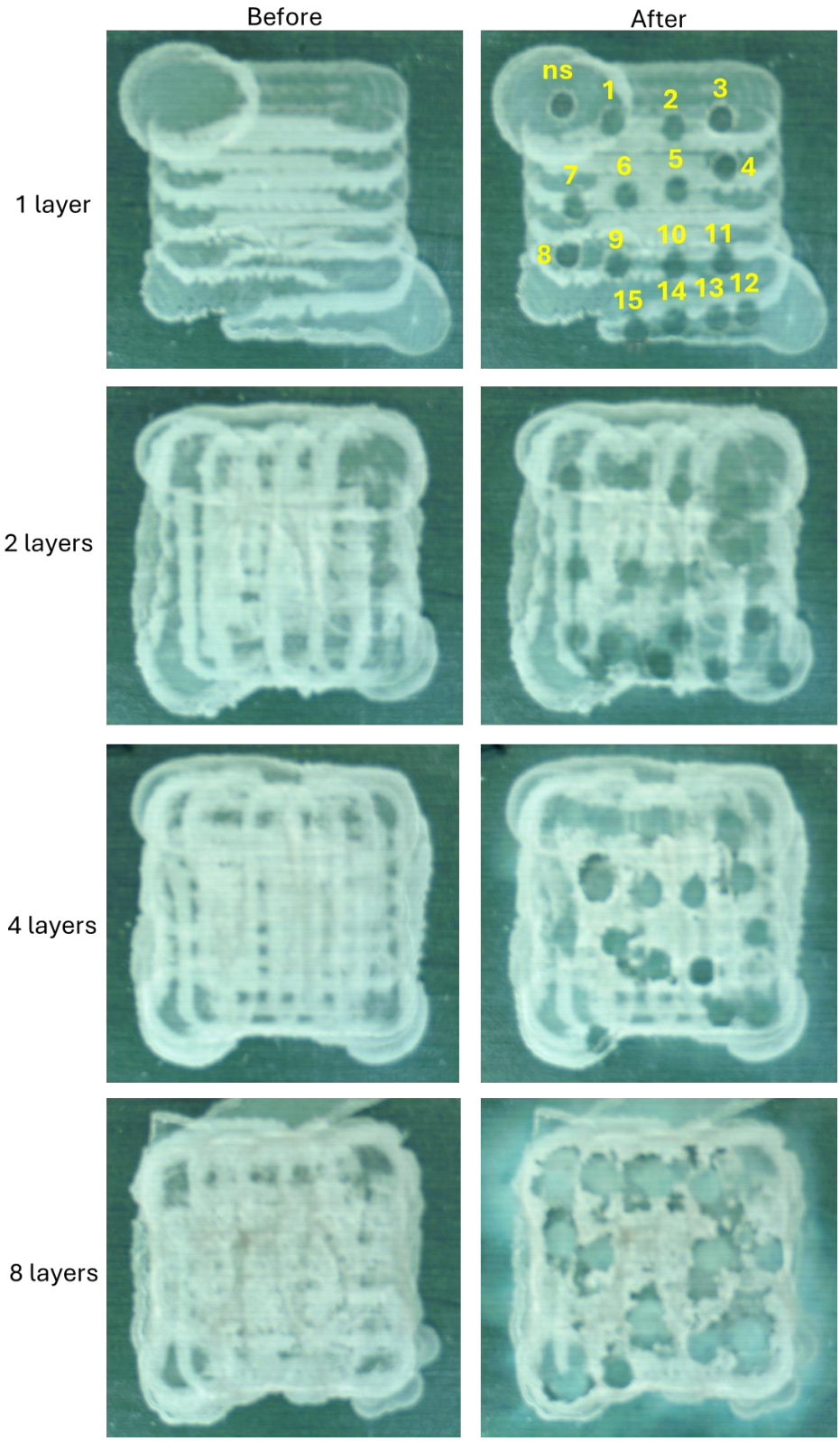

Figure 3. Microscope images of the A-square AP + CuO samples before (left) and after (right) LASEM measurements; the high-speed video number is indicated for the one-layer sample. ns = not saved.

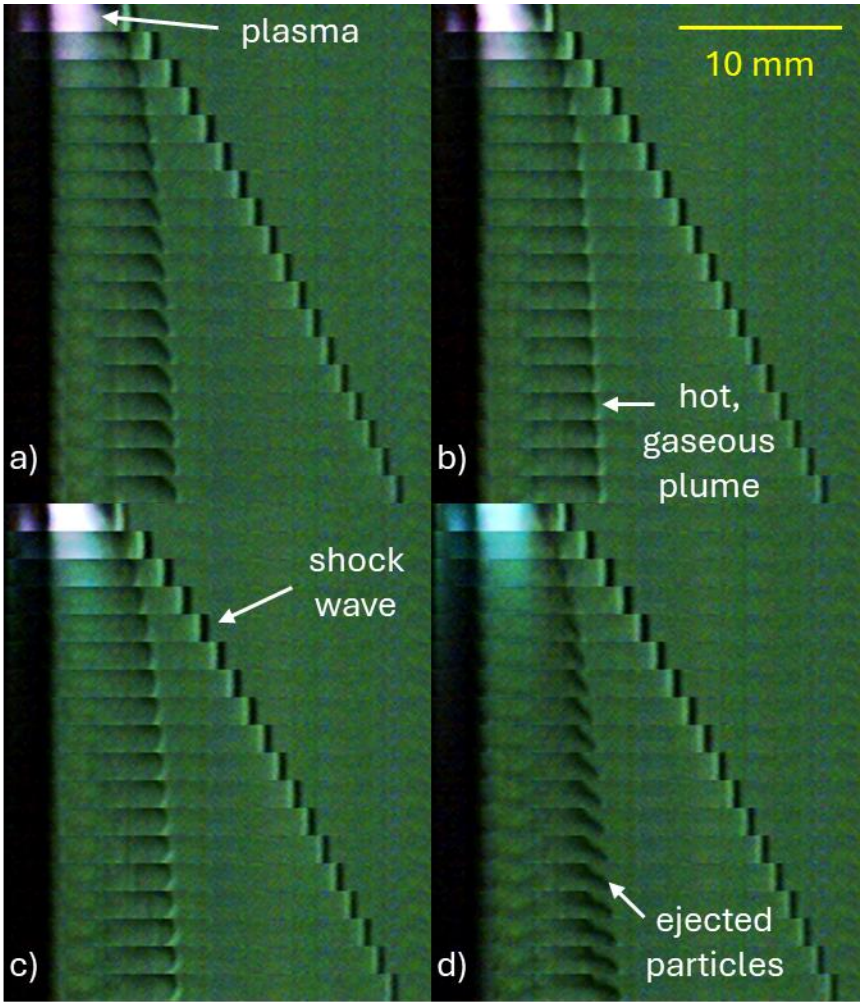

Figure 4. Snapshots from the high-speed schlieren video for a) 1layerA, b) 2layerA, c) 4layerA, and d) 8layerA. The images have been rotated 90° and cropped with brightness increased by 80%.

The plume heights at 161.9 μs (the last saved camera frame) were measured for each video and are shown for each sample batch in Figure 5. The average plume heights increase with increasing sample layers, indicating more material is reacting in the air above the sample surface during this timeframe. While the 95% confidence intervals (CIs) for the two batches overlap significantly for each sample, they are also larger for the four- and eight-layer samples, indicating the stochastic nature of the amount of ejected material per laser shot.

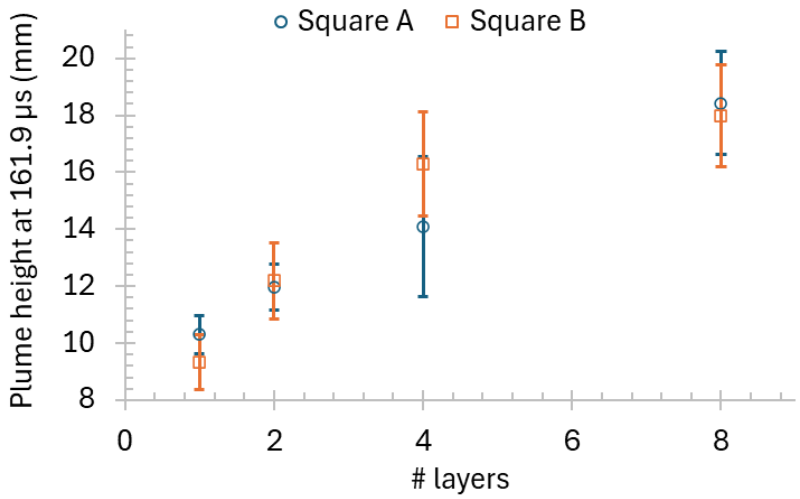

Figure 5. Average plume height at 161.9 µs as a function of the number of printed AP + CuO layers. Error bars indicate 95% CIs.

The time-resolved IR emission traces demonstrate that the additional blowoff with increasing number of layers increases the amount of post-plasma combustion on the hundreds of microseconds timescale (Figure 6). Shaded regions indicate the 95% CIs based on the data saved for five laser shots per sample. The one- and two-layer signals overlap significantly, with the four-layer sample showing slightly higher post-plasma combustion. The eight-layer sample has, by far, the most significant post-plasma combustion.

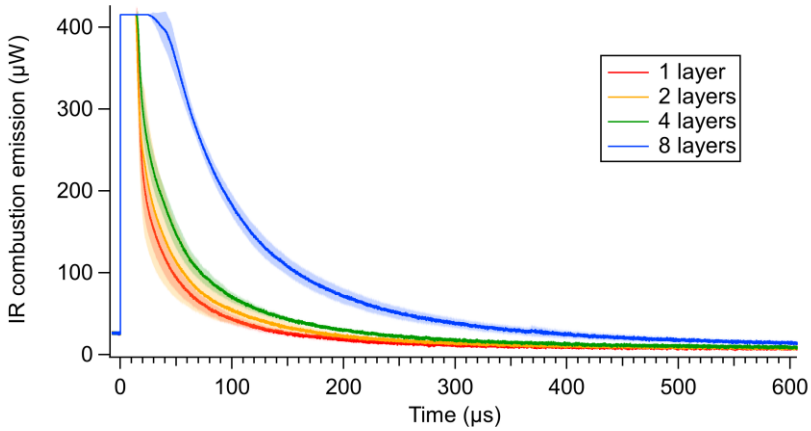

Figure 6. Time-resolved IR emission for each sample. Shaded regions indicate the 95% CIs.

A single-shot emission spectrum from the laser-induced plasma was obtained with every laser shot. The averaged spectra for each sample thickness are shown in Figure 7. Dominant emission features include the following: silicon (Si), magnesium (Mg), calcium (Ca), potassium (K), and sodium (Na) from the glass slide; oxygen (O) from a combination of entrained air, the slide, and the sample; nitrogen (N) from the air and sample; iron (Fe) and K contamination in the sample

(on the order of a few parts-per-million); and carbon (C), Cu, hydrogen (H), and chlorine (Cl) from the sample and residual solvent. Significant emission from the slide appears in the spectra for the one- and two-layer samples, indicating poorer surface coverage for the printed sample. Emission lines from the sample increase in intensity with increasing printed layers—except for the Cl lines, which decrease in intensity with increasing layers. This could indicate increasing Cl reactivity with larger amounts of ablated material in the plasma, or a decrease in sample homogeneity with increasing layers (i.e., less AP). Figure 8 summarizes the background-corrected peak emission intensities for each sample (color-coded by primary origin).

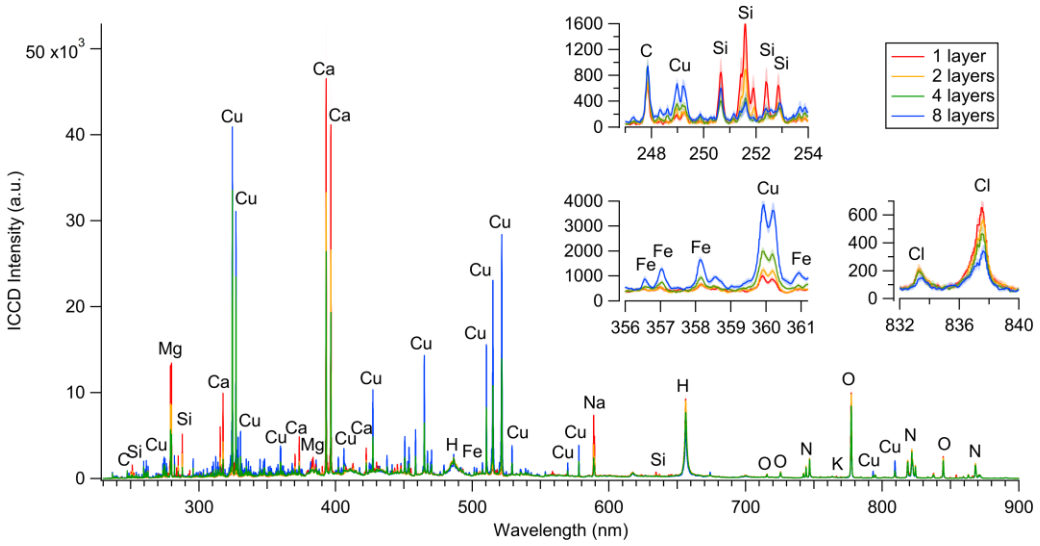

Figure 7. Laser-induced plasma emission spectra averaged over all sample shots for each layer thickness. Shaded regions indicate 95% CIs. Dominant emission features have been labelled. Insets provide additional detail for weaker emission features.

Figure 8. Background-corrected peak emission intensities for each sample (color-coded by primary origin).

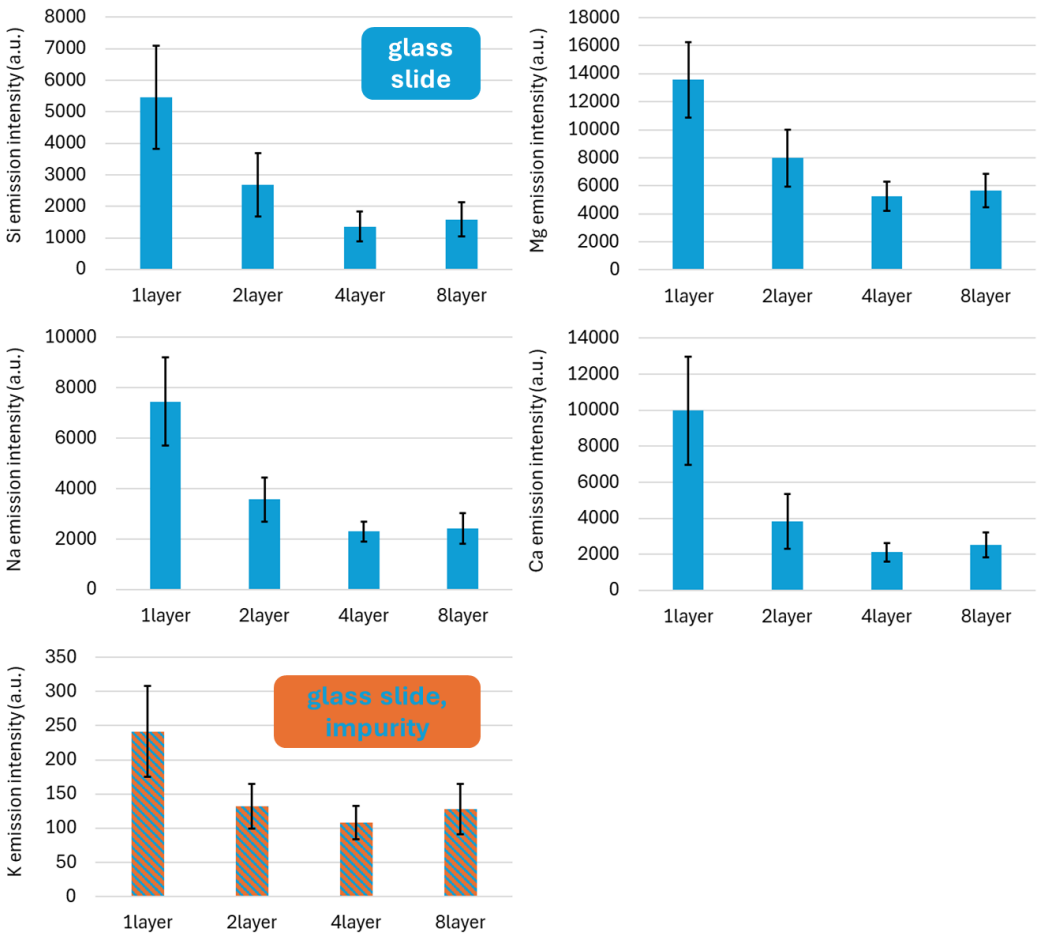

Figure 8. Background-corrected peak emission intensities for each sample (color-coded by primary origin) (continued).

The sample homogeneity was investigated by comparing the 95% CIs for the plasma spectra calculated based on the single-shot data (Figure 9). Overall, the 95% CIs were less significant than expected and decreased as the number of layers increased (indicating increased shot-to-shot reproducibility), up to four layers. At 8 layers, the 95% CIs increased slightly (with an average value of 58 compared with 48 for the 4-layer sample). Most of the variability in the one- and two-layer samples resulted from the emission features related to the slide—i.e., whether the laser hit a more transparent region with less material. At larger sample thicknesses, the sample homogeneity contributes more to the variability. The shot-to-shot variability of the two- and four-layer samples are similar.

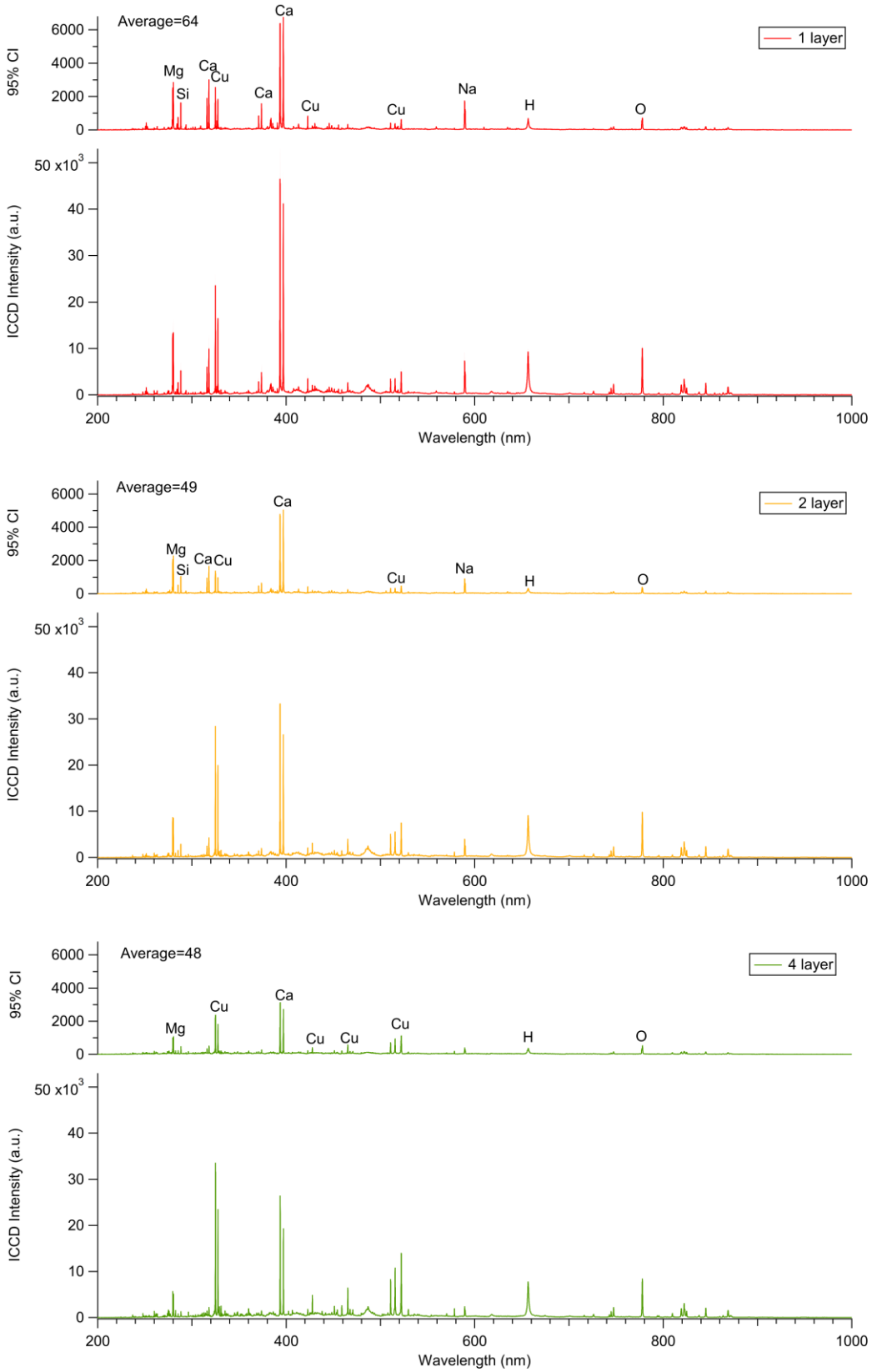

Figure 9. Shot-to-shot variability in the laser-induced plasma spectra.

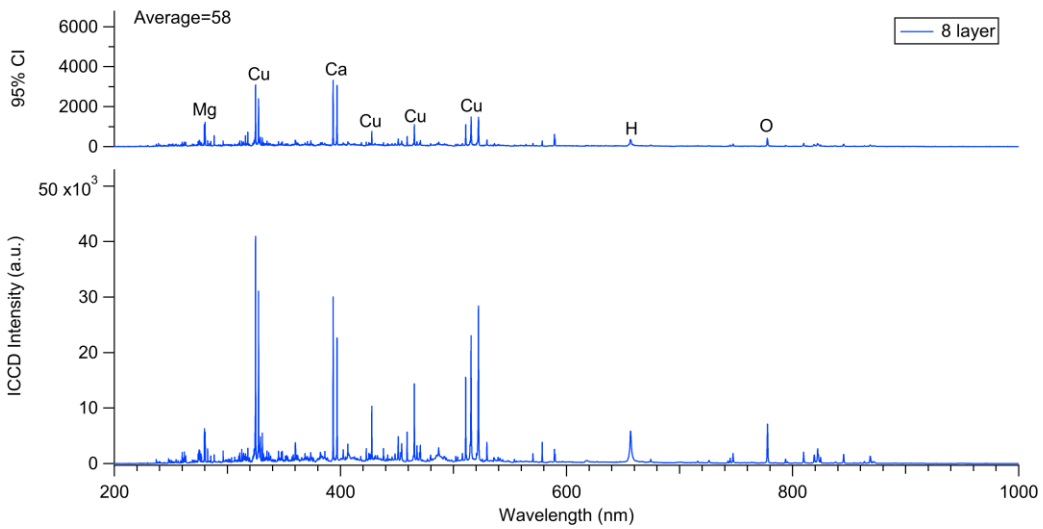

Figure 9. Shot-to-shot variability in the laser-induced plasma spectra (continued).

The laser-induced plasma excitation temperatures based on the relative intensities of five atomic Cu lines (427.51, 465.11, 510.55, 515.32, and 521.82 nm) were calculated using the Boltzmann plot method (Figure 10). While no significant differences in plasma temperatures were observed, there was a slight increase in average temperature with increasing number of layers. The 95% CIs for the one-layer sample were higher because of poorer signal-to-noise ratio for the Cu lines. The average temperatures for the two- and four-layer samples were nearly identical.

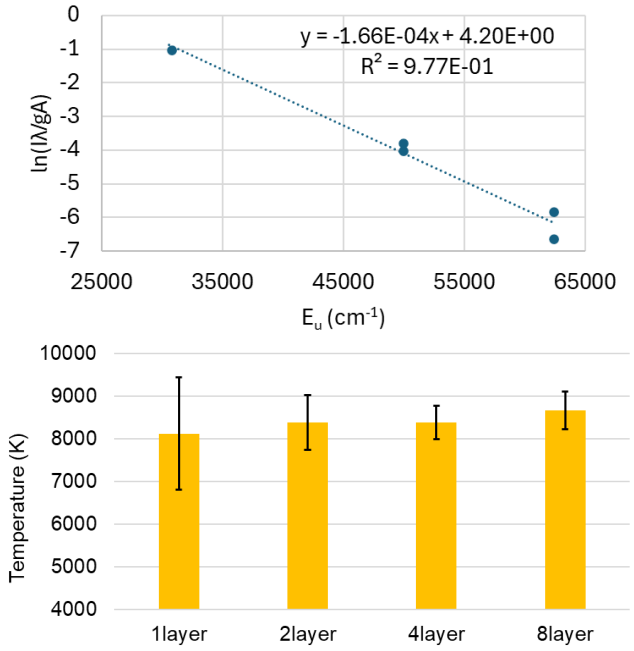

Figure 10. Example Boltzmann plot (top) and average laser-induced plasma excitation temperatures based on the relative intensities of Cu emission lines (bottom). Error bars indicate 95% CIs.

The characteristic laser-induced shock velocities, determined by fitting the combined sample sets as well as the averaged data for each sample square, are shown in Figure 11. Only the eight-layer sample had identical results for both squares, but the average values for the other samples are within the 95% CIs. The characteristic laser-induced shock velocities increase with increasing number of layers, indicating that the ablation of the glass slide into the laser-induced plasma dilutes the energy release; while some contribution to the increase may be due to larger amounts of the AP + CuO sample ablated into the laser-induced plasma, the increase for other energetic samples prepared on double-sided tape was previously observed to be minor.[13] For detonable energetic materials, the characteristic laser-induced shock velocities are directly correlated to the detonation velocity of the material at large scale[2] and are thus indicative of the early, single-digit microsecond timescale energy release.

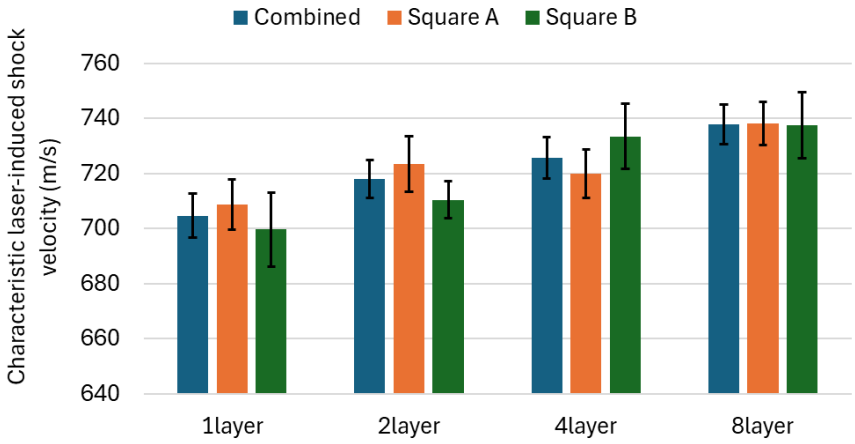

Figure 11. Characteristic laser-induced shock velocities for the combined sample shots vs. shots obtained from squares A or B. Error bars indicated 95% CIs.

Figure 12 shows the correlation between the characteristic laser-induced shock velocities and the Dewey shock velocities. For materials such as aluminized explosives that have late-reacting components, the increase in Dewey shock velocity exceeds the increase in characteristic laser-induced shock velocity since more energy is released later in the plasma lifetime. For the AP + CuO samples, the increase in both parameters is close to linear (dotted yellow line). The values from a previous study[14] for neat AP (200 μm) powder affixed to a glass slide after drying are shown for comparison. Both the characteristic laser-induced shock velocities and Dewey shock velocities are higher for the AP + CuO samples than for neat AP, consistent with the expectation of faster AP decomposition and larger energy release in the presence of the CuO catalyst. The larger Dewey shock velocity for the four-layer sample compared with the two-layer sample suggests combustion

from ejected particles does partially contribute to the total energy release in the laser-induced plasma.

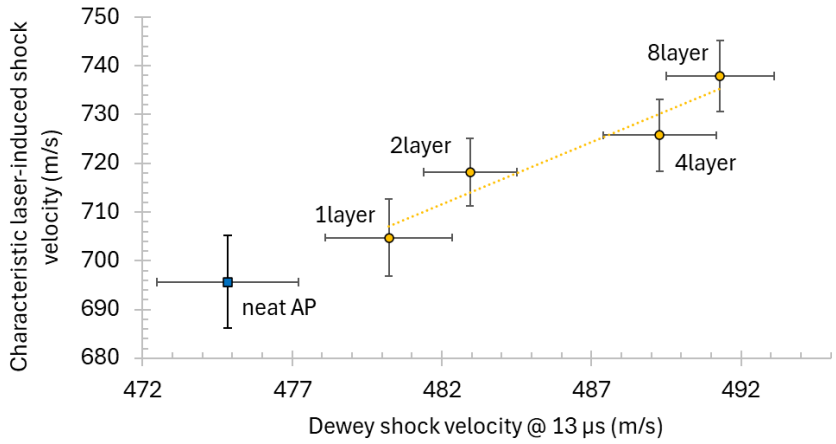

Figure 12. Correlation between the early time energy release (characteristic laser-induced shock velocity extrapolated to time zero) and the late time energy release in the plasma (Dewey shock velocity at 13 µs) for neat 200 µm AP (blue square)[14] and the printed AP + CuO samples (yellow diamonds).

Multiple comparison of means testing was performed on the AP + CuO data set to determine if the differences in mean values were statistically significant for each sample. Figure 13 shows a graphical illustration of the results for the characteristic laser-induced shock velocities. The red markers indicate the means are statistically different from the 1layerA sample (square A on the one-layer slide) at the 95% confidence level, while the gray markers are not (i.e., the CI bands overlap). Thus, there is no significant difference in characteristic laser-induced velocities for squares A or B for the one-layer sample. The same is true for all four samples. The full results are shown in Figure 14a, where p-values < 0.05 are shaded in red or orange and indicate the means are statistically significant at the 95% confidence level. Figure 14b shows the multiple comparison of means test results for the Dewey shock velocities, which show the same trend. The Sedov–Taylor energies added to the plasma (Figure 14c) also showed similar trends. Table 2 lists the results for the combined LASEM parameters and individual sample batches.

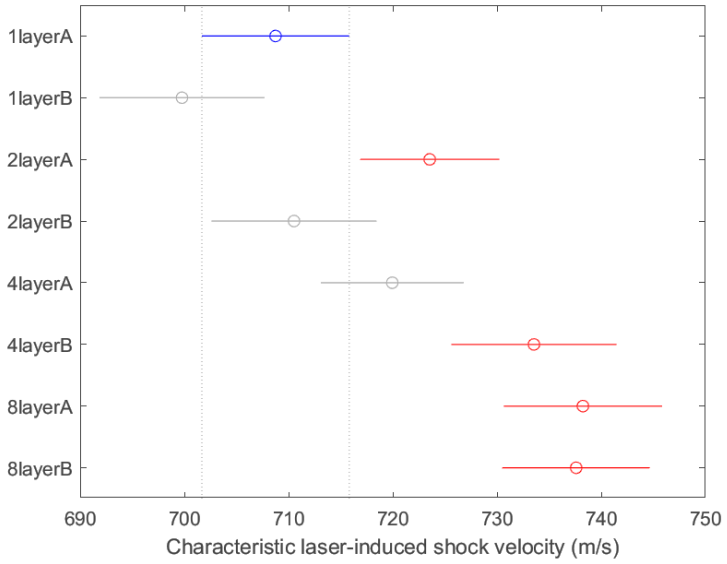

Figure 13. Multiple comparison of means test results for the characteristic laser-induced shock velocities.

a)	**1layerA**	**1layerB**	**2layerA**	**2layerB**	**4layerA**	**4layerB**	**8layerA**	**8layerB**
1layerA		2.4E-01	3.5E-02	8.2E-01	1.1E-01	1.4E-03	1.2E-04	1.0E-04
1layerB	2.4E-01		1.7E-03	1.8E-01	8.0E-03	4.9E-05	3.2E-06	2.3E-06
2layerA	3.5E-02	1.7E-03		8.0E-02	6.0E-01	1.8E-01	4.4E-02	4.5E-02
2layerB	8.2E-01	1.8E-01	8.0E-02		2.1E-01	4.7E-03	5.9E-04	5.2E-04
4layerA	1.1E-01	8.0E-03	6.0E-01	2.1E-01		7.1E-02	1.4E-02	1.3E-02
4layerB	1.4E-03	4.9E-05	1.8E-01	4.7E-03	7.1E-02		5.5E-01	5.9E-01
8layerA	1.2E-04	3.2E-06	4.4E-02	5.9E-04	1.4E-02	5.5E-01		9.3E-01
8layerB	1.0E-04	2.3E-06	4.5E-02	5.2E-04	1.3E-02	5.9E-01	9.3E-01	
b)	**1layerA**	**1layerB**	**2layerA**	**2layerB**	**4layerA**	**4layerB**	**8layerA**	**8layerB**
1layerA		7.6E-02	1.5E-01	3.5E-01	2.9E-04	1.6E-05	1.3E-05	3.1E-04
1layerB	7.6E-02		1.8E-03	1.1E-02	5.3E-07	2.9E-08	2.2E-08	6.2E-07
2layerA	1.5E-01	1.8E-03		7.0E-01	1.8E-02	1.3E-03	1.3E-03	1.8E-02
2layerB	3.5E-01	1.1E-02	7.0E-01		1.1E-02	9.2E-04	8.9E-04	1.1E-02
4layerA	2.9E-04	5.3E-07	1.8E-02	1.1E-02		2.9E-01	3.1E-01	9.7E-01
4layerB	1.6E-05	2.9E-08	1.3E-03	9.2E-04	2.9E-01		9.5E-01	3.1E-01
8layerA	1.3E-05	2.2E-08	1.3E-03	8.9E-04	3.1E-01	9.5E-01		3.3E-01
8layerB	3.1E-04	6.2E-07	1.8E-02	1.1E-02	9.7E-01	3.1E-01	3.3E-01	
c)	**1layerA**	**1layerB**	**2layerA**	**2layerB**	**4layerA**	**4layerB**	**8layerA**	**8layerB**
1layerA		8.8E-01	3.7E-01	9.1E-02	4.1E-02	5.9E-03	1.4E-02	1.2E-02
1layerB	8.8E-01		4.9E-01	1.4E-01	7.5E-02	1.3E-02	2.9E-02	2.6E-02
2layerA	3.7E-01	4.9E-01		3.7E-01	2.3E-01	4.5E-02	9.3E-02	8.6E-02
2layerB	9.1E-02	1.4E-01	3.7E-01		8.3E-01	3.0E-01	4.8E-01	4.8E-01
4layerA	4.1E-02	7.5E-02	2.3E-01	8.3E-01		3.7E-01	5.9E-01	6.0E-01
4layerB	5.9E-03	1.3E-02	4.5E-02	3.0E-01	3.7E-01		7.2E-01	6.9E-01
8layerA	1.4E-02	2.9E-02	9.3E-02	4.8E-01	5.9E-01	7.2E-01		9.8E-01
8layerB	1.2E-02	2.6E-02	8.6E-02	4.8E-01	6.0E-01	6.9E-01	9.8E-01	

Figure 14. Multiple comparison of means results (p-values) for the a) characteristic laser-induced shock velocities, b) Dewey shock velocities, and c) Sedov–Taylor energies. Red shading indicates means are statistically different at greater than the 95% confidence level ($p < 0.05$). Green shading indicates no significant difference.

Table 2. Calculated parameters from the SR-LASEM results for the sample averages (over squares A and B), square A, or square B.

Sample	Characteristic laser-induced shock velocity (m/s)	95% CI	Dewey shock velocity (m/s)	95% CI	Sedov–Taylor energy (mJ)	95% CI
1layer	704.76	7.92	480.23	2.12	6.73	0.31
2layer	718.16	6.89	482.94	1.56	9.91	0.39
4layer	725.78	7.40	489.28	1.89	13.05	0.52
8layer	737.90	7.27	491.30	1.81	13.40	0.61
1layerA	708.75	9.25	480.09	2.24	6.54	0.37
2layerA	723.54	10.13	483.92	2.30	8.89	0.41
4layerA	719.95	8.71	485.26	2.14	11.97	0.39
8layerA	738.24	7.82	490.62	2.46	13.44	0.55
1layerB	699.77	13.48	480.52	3.69	6.97	0.43
2layerB	710.52	6.73	487.21	2.01	11.36	0.54
4layerB	733.54	11.77	491.14	3.38	14.48	0.57
8layerB	737.59	12.02	491.94	2.61	13.36	0.63

4. Conclusions

SR-LASEM was demonstrated on printed energetic materials for the first time. For the provided samples, it was found that 12–16 laser shots could be obtained on each roughly 10-mm square batch—thus, a minimum of 2 squares are needed to obtain sufficient replicate shots (minimum of 20 desired). The use of multiple squares also ensures that the batch-to-batch variability can be determined. For the current set of samples, no statistically significant differences were observed between the two batches of each sample.

This study confirmed that for the one-layer sample, significant amounts of the glass slide used as the substrate for the printed materials were ablated into the plasma, resulting in emission features from the slide and lower energy releases. At the other extreme, eight-layer samples resulted in significant sample blowoff with each laser shot, which made it more challenging to obtain a sufficient number of nonoverlapping laser shots and significantly increased the observed post-plasma combustion reactions as the ejected material ignited in the air.

The two- and four-layer samples had the closest characteristic laser-induced shock velocities (i.e., fast energy release on the microsecond timescale) and calculated plasma excitation temperatures. In addition, the shot-to-shot variability was lowest for those two samples. However, the two-layer sample had more significant emission from the slide while the four-layer sample had better signal-to-noise ratios for the emission features produced by the AP + CuO. For these reasons, the four-layer sample is the recommended sample thickness for LASEM measurements—although the two-layer sample would be acceptable if shorter printing times or less

material expenditure is necessary. If the primary interest is on the later timescale combustion reactions, thicker samples (eight layers or more) are better.

Overall, the shot-to-shot reproducibility for the printed AP + CuO samples is as good or slightly better than our typical sample preparation (loose powder affixed to double-sided tape), despite the obvious visual inhomogeneity in sample deposition. The laser-material interaction is inherently stochastic and the error bars for the shock velocity versus time data can be significant; here, any minor variability from the observed sample inhomogeneity is smaller than the error bars of the measurement. However, significant variability resulting from multiple materials with different energetic content has been observed for other inhomogeneous samples.[2]

5. References

1. Gottfried JL, Barnes BC. Spatially resolved laser-induced air shock from energetic material (SR-LASEM) measurements, part I: plasma-enhanced chemical vapor deposition films. DEVCOM Army Research Laboratory (US); 2026 Forthcoming.

2. Gottfried JL, Wainwright ER. Laser-induced air shock from energetic materials (LASEM): a novel microscale technique for characterizing energy release at high heating rates. J Energ Mater. 2023;43(1):1–61.

3. Demko AR, Lajoie JA, Thomas AR, Ramirez DJ, Sippel TR. Impacts of metal oxide crystalline structure on the decomposition of solid propellants under combustion heating rates. Fuel Commun. 2024;19:100112.

4. Ji H et al. Study on the catalytic effect of nano copper oxide with different particle sizes on the thermal decomposition of ammonium perchlorate. Catalysts. 2025;15:882.

5. Muravyev NV, Monogarov KA, Schaller U, Fomenkov IV, Pivkina AN. Progress in additive manufacturing of energetic materials: creating the reactive microstructures with high potential of applications. Propellants Explos Pyrotech. 2019;44(8):941–969.

6. Zong HZ et al. Energetic materials in 3D: an in-depth exploration of additive manufacturing techniques. Int J Adv Manuf Technol. 2024;133:3059–3080.

7. Kalman J. California State University, Long Beach. Personal communication, 2026 Feb 17.

8. Saeidi M. California State University, Long Beach. Personal communication, 2026 Mar 9.

9. Gottfried JL, Dillier CAM, Wainwright ER. Automated shock wave measurement and fitting for the LASEM-420 system, part I: description of MATLAB codes. DEVCOM Army Research Laboratory (US); 2023 Aug. Report No.: ARL-TR-9738.

10. Gottfried JL, Dillier CAM, Wainwright ER. Automated shock wave measurement and fitting for the LASEM-420 system, part II: comparison of explosive data. DEVCOM Army Research Laboratory (US); 2023 Aug. Report No.: ARL-TR-9756.

11. Gottfried JL. Automated shock wave measurement and fitting for the LASEM-420 system, part III: influence of pixel rounding errors. DEVCOM Army Research Laboratory (US); 2023 Dec. Report No.: ARL-TN-1184.

12. Gottfried JL. Automated shock wave measurement and fitting for the LASEM-420 system, part IV: statistical significance of calculated parameters. DEVCOM Army Research Laboratory (US); 2024 Nov. Report No.: ARL-TN-1233.

13. Gottfried JL, Smith DK, Wu C-C, Pantoya ML. Improving the explosive performance of aluminum nanoparticles with aluminum iodate hexahydrate (AIH). Sci Rep. 2018;8:8036.

14. Gottfried JL, Dillier CA, Pesce-Rodriguez R, Wainwright ER, Giri L. Influence of formulation ingredients on aluminum reactivity, part I: particle size effects for ammonium perchlorate stimulated at high heating rates. DEVCOM Army Research Laboratory (US); 2024 May. Report No.: ARL-TR-9910.

List of Symbols, Abbreviations, and Acronyms

3D	Three-Dimensional
AP	Ammonium Perchlorate
ARL	Army Research Laboratory
C	Carbon
Ca	Calcium
CI	Confidence Interval
Cl	Chlorine
Cu	Copper
CuO	Copper(II) Oxide
DEVCOM	U.S. Army Combat Capabilities Development Command
Fe	Iron
H	Hydrogen
ICCD	Intensified Charge-Coupled Device
IR	Infrared
K	Potassium
LASEM	Laser-Induced Air Shock from Energetic Materials
Mg	Magnesium
N	Nitrogen
Na	Sodium
O	Oxygen
PVP	Polyvinylpyrrolidone
Si	Silicon
SR-LASEM	Spatially Resolved Laser-Induced Air Shock from Energetic Materials
UV	Ultraviolet

1 (PDF)	DEFENSE TECHNICAL INFORMATION CTR DTIC OCA
1 (PDF)	DEVCOM ARL FCDD RLB CB TECH LIB